Article

Locating the sets of exceptional points in dissipative systems and the self-stability of bicycles

Oleg Kirillov [1]

[1] Northumbria University, Newcastle upon Tyne, NE1 8ST, United Kingdom; oleg.kirillov@northumbria.ac.uk

Version June 28, 2018 submitted to Entropy

Abstract: Sets in the parameter space corresponding to complex exceptional points have high codimension and by this reason they are difficult objects for numerical location. However, complex EPs play an important role in the problems of stability of dissipative systems where they are frequently considered as precursors to instability. We propose to locate the set of complex EPs using the fact that the global minimum of the spectral abscissa of a polynomial is attained at the EP of the highest possible order. Applying this approach to the problem of self-stabilization of a bicycle we find explicitly the EP sets that suggest scaling laws for the design of robust bikes that agree with the design of the known experimental machines.

Keywords: Exceptional points in classical systems, coupled systems, non-holonomic constraints, nonconservative forces, stability optimization, spectral abscissa, swallowtail, bicycle self-stability

1. Introduction

Exceptional points in classical systems have recently attracted attention of researchers in the context of the parity-time (PT) symmetry found in mechanics [1,2] and electronics [3]. In the context of stability of classical systems the PT-symmetry plays a part in systems of coupled mechanical oscillators with the indefinite matrix of damping forces [4–8]. Stable PT-symmetric indefinitely damped mechanical systems have imaginary eigenvalues and thus form singularities on the boundary of the domain of asymptotic stability of general dissipative systems [9,10]. Among these singularities are exceptional points corresponding to double imaginary eigenvalues with the Jordan block. They belong to sets of complex exceptional points with nonzero real parts that live both in the domain of instability and in the domain of asymptotic stability of a dissipative system and pass through the imaginary exceptional points on the stability boundary that bound the region of PT-symmetry [11,12]. These are sets of high codimension which are hard to find by numerical approaches. Nevertheless, in many applications it was realized that complex exceptional points hidden inside the domain of asymptotic stability significantly influence the transition to instability [13,14]. How to locate the set of complex exceptional points? The general approach involving commutators of matrices of the system [15,16] does not look easily interpretable. In this paper we will use a recent observation [17] that the set of complex exceptional points connects the imaginary exceptional points on the boundary of asymptotic stability and the real exceptional points inside the domain of asymptotic stability that lie on the boundary of the domain of heavy damping. We will show how location of the exceptional points with this approach helps to find explicit scaling laws in the classical problem of self-stability of bicycles.

2. Complex exceptional points and the self-stability of bicycles

Bicycle is easy to ride but surprisingly difficult to model [18]. Refinement of the mathematical model of a bicycle continues over the last 150 years with contributions from Rankine, Boussinesq,

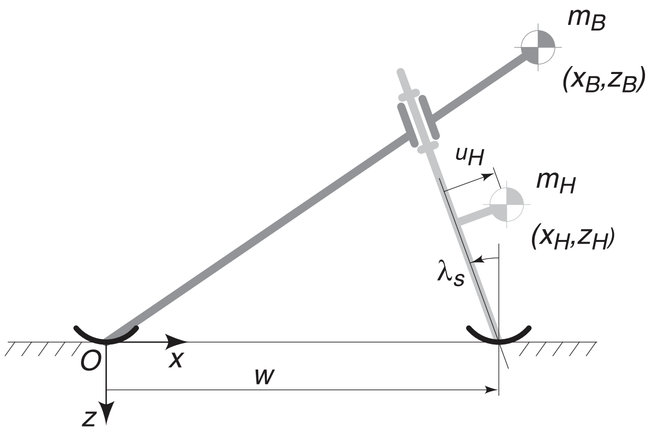

Figure 1. The two-mass-skate (TMS) bicycle model [27].

Whipple, Klein, Sommerfeld, Appel, Synge and many others [19–21]. A canonical, commonly accepted nowadays model goes back to the 1899 work by Whipple. The Whipple bike is a system consisting of four rigid bodies with knife-edge wheels making it non-holonomic, i.e. requiring for its description more configuration coordinates than the number of its admissible velocities [22,23]. Due to the non-holonomic constraints even the bicycle tire tracks have a nontrivial and beautiful geometry that has deep and unexpected links to integrable systems, particle traps, and the Berry phase [24–26].

A fundamental empirical property of real bicycles is their self-stability without any control at a sufficiently high speed [27]. This property has a number of important practical implications. For instance, recent experiments confirm the long-standing assumption that the bicycle designs that do not present the self-stability are difficult for a person to ride, in other words more stable bikes handle better [18,28]. Hence, deeper understanding of the passive stabilization can provide new principles for the design of more safe and rideable bicycles, including compact and foldable models. Furthermore, it is expected to play a crucial part in formulating principles of design of energy-efficient wheeled and bipedal robots [29].

However, the theoretical explanation of the self-stability has been highly debated throughout the history of bicycle dynamics [22] to such an extent that a recent news feature article in Nature described this as “the bicycle problem that nearly broke mathematics” [18]. An excellent scientific and historical review of thoughts on the bicycle self-stability can be found in [21].

The reason to why “simple questions about self-stabilization of bicycles do not have straightforward answers” [20] lies in the symbolical complexity of the Whipple model that contains 7 degrees of freedom and depends on 25 physical and design parameters [19]. In recent numerical simulations [19,20,22] self-stabilization has been observed for some benchmark designs of the Whipple bike. These results suggested further simplification of the model yielding a reduced model of a bicycle with vanishing radii of the wheels (that are replaced by skates, see e.g. [30]), known as the two-mass-skate (TMS) bicycle [27,28]. Despite the self-stable TMS bike has been successfully realized in the recent laboratory experiments [27], its self-stability still waits for a theoretical explanation.

In the following, we will show how location of complex and real exceptional points allows to find hidden symmetries in the model suggesting further reduction of the parameter space and, finally, providing explicit relations between the parameters of stability-optimized TMS bikes.

2.1. The TMS bicycle model

The TMS model is sketched in Fig. 1. It depends on 9 dimensional parameters:

$$w, \quad v, \quad \lambda_s, \quad m_B, \quad x_B, \quad z_B, \quad m_H, \quad x_H, \quad z_H$$

Table 1. Notation for the TMS bicycle model

Dimensional	Meaning	**Dimensionless**	Meaning
v	Velocity of the bike		
g	Gravity acceleration	Fr	Froude number
w	Wheel base		
λ_s	Steer axis tilt (rad.)	λ_s	Steer axis tilt (rad.)
m_H	Front fork and handlebar assembly (FHA) mass	μ	Mass ratio (m_H/m_B)
m_B	Rear frame assembly (RFA) mass		
x_H (≥ 0)	Horizontal coordinate of the FHA centre of mass	χ_H (≥ 0)	Horizontal coordinate of the FHA centre of mass
z_H (≤ 0)	Vertical coordinate of the FHA centre of mass	ζ_H (≤ 0)	Vertical coordinate of the FHA centre of mass
x_B (≥ 0)	Horizontal coordinate of the RFA centre of mass	χ_B (≥ 0)	Horizontal coordinate of the RFA centre of mass
z_B (≤ 0)	Vertical coordinate of the RFA centre of mass	ζ_B (≤ 0)	Vertical coordinate of the RFA centre of mass
t	Time	τ	Time

that represent, respectively, the wheel base, velocity of the bicycle, steer axis tilt, rear frame assembly (B) mass, horizontal and vertical coordinates of the rear frame assembly centre of mass, front fork and handlebar assembly (H) mass, and horizontal and vertical coordinates of the front fork and handlebar assembly centre of mass [27], see Table 1.

We wish to study stability of the TMS bicycle that is moving along a straight horizontal trajectory with the constant velocity and remaining in a straight vertical position. In order to simplify the analysis it is convenient to choose the wheelbase, w, as a unit of length and introduce the dimensionless time $\tau = t\sqrt{\frac{g}{w}}$ and 7 dimensionless parameters

$$\mathrm{Fr} = \frac{v}{\sqrt{gw}}, \quad \mu = \frac{m_H}{m_B}, \quad \chi_B = \frac{x_B}{w}, \quad \chi_H = \frac{x_H}{w}, \quad \zeta_B = \frac{z_B}{w}, \quad \zeta_H = \frac{z_H}{w}, \quad \lambda_s,$$

where g is the gravity acceleration, Fr the Froude number and μ the mass ratio, see Table 1. Notice that $\zeta_B \leq 0$ and $\zeta_H \leq 0$ due to choice of the system of coordinates, Fig. 1.

It has been shown in [19,27] that small deviations from the straight vertical equilibrium of the TMS bicycle are described by the leaning angle, ϕ, of the frame and the steering angle, δ, of the front wheel/skate. These angles are governed by the two coupled linear differential equations

$$\mathbf{M}\ddot{\mathbf{q}} + \mathbf{V}\dot{\mathbf{q}} + \mathbf{P}\mathbf{q} = 0, \quad \mathbf{q} = (\phi, \delta)^T, \tag{1}$$

where dot denotes differentiation with respect to dimensionless time, τ, and the matrices of mass, $\mathbf{M}$, velocity-dependent forces, $\mathbf{V}$, and positional forces, $\mathbf{P}$, are

$$\mathbf{M} = \begin{pmatrix} \mu\zeta_H^2 + \zeta_B^2 & -\mu\zeta_H\nu_H \\ -\mu\zeta_H\nu_H & \mu\nu_H^2 \end{pmatrix}, \quad \mathbf{V} = \begin{pmatrix} 0 & -\mu\chi_H\zeta_H - \chi_B\zeta_B \\ 0 & \mu\chi_H\nu_H \end{pmatrix} \mathrm{Fr}\cos\lambda_s,$$
$$\mathbf{P} = \begin{pmatrix} \mu\zeta_H + \zeta_B & -\mathrm{Fr}^2\cos\lambda_s(\mu\zeta_H + \zeta_B) - \mu\nu_H \\ -\mu\nu_H & \mu(\mathrm{Fr}^2\cos\lambda_s - \sin\lambda_s)\nu_H \end{pmatrix}, \tag{2}$$

respectively, with $\nu_H = \frac{u_H}{w} = (\chi_H - 1)\cos\lambda_s - \zeta_H\sin\lambda_s$, see Fig. 1.

2.2. Preliminaries on Lyapunov stability and asymptotic stability of equilibria

An equilibrium of a nonlinear dynamical system is said to be *Lyapunov stable* if all the solutions starting in its vicinity remain in some neighborhood of the equilibrium in the course of time [17,31,32]. For *asymptotic stability*, the solutions are required, additionally, to converge to the equilibrium as time tends to infinity. The first (indirect) method of Lyapunov reduces the study of asymptotic stability of an *autonomous* (time-independent) system to the problem of location in the complex plane of eigenvalues of the operator of its *linearization* [31]. In a finite-dimensional case the eigenvalues are roots of a *polynomial characteristic equation*. Localization of all the roots in the open left half of the complex plane is a necessary and sufficient condition for asymptotic stability of a linearization, which usually implies asymptotic stability of the original non-linear system [31]. The algebraic Routh-Hurwitz criterion provides explicit conditions for asymptotic stability expressed in terms of the coefficients of the characteristic polynomial [32]. The Lienard-Chipart criterion is an equivalent version of the Routh-Hurwitz criterion, which sometimes gives simpler expressions for the stability conditions [32].

Solution to the linear differential equation is a linear combination of exponential functions with the argument equal to time multiplied with an eigenvalue. Consequently, in the domain of asymptotic stability solutions of the linearization exponentially decay in time either with oscillations, which corresponds to a complex eigenvalue with the negative real part, or without oscillations, which corresponds to a negative real eigenvalue. If all the solutions exponentially decay without oscillations, i.e. all eigenvalues are real and negative, the system is said to be *heavily damped* [32,36,37]. A perturbed heavily damped system quickly and monotonously returns to its equilibrium which is percepted by an observer as a robust stability. By this reason placement of parameters of a system into the domain of heavy damping is a desirable goal in many engineering applications [36,37]. Naturally, heavy damping implies asymptotic stability and therefore the domain of heavy damping belongs to the domain of asymptotic stability in the parameter space [17].

Similarly, in the domain of instability a complex eigenvalue with the positive real part corresponds to an oscillatory solution with the exponentially growing amplitude. This unstable behavior is frequently called flutter, dynamic instability, oscillatory instability or Hopf bifurcation in different engineering and physical contexts [32]. In the context of bicycle dynamics the growing oscillations are referred to as the *weaving* instability [19,20]. A positive real eigenvalue corresponds to the static instability (or steady-state bifurcation) of an equilibrium described by a non-oscillatory solution with an exponentially growing amplitude. A bicycle is *capsizing* in this case [19,20].

With the change of parameters of the system one can move from the domain of instability to the domain of asymptotic stability in the parameter space. This transition is accompanied by the crossing of the imaginary axis in the complex plane either by at least one pair of complex-conjugate simple eigenvalues or by at least one real eigenvalue. Exactly on the stability boundary the eigenvalues become imaginary or zero, respectively. In multiple parameter systems multiple imaginary or zero eigenvalues with different algebraic and geometric multiplicities are generically possible on the stability boundary. In physics, a point in the parameter space corresponding to a linear operator (matrix, matrix polynomial) with the multiple eigenvalue that has less eigenvectors than its algebraic multiplicity[1] is called an *exceptional point*.[2] Exceptional points form geometric singularities both on the boundary of asymptotic stability and on the boundary of the domain of heavy damping [17,32]. Moreover, exceptional points corresponding to complex eigenvalues exist inside both the domain of asymptotic stability and the domain of instability. Below we uncover all the exceptional points in the TMS bicycle model and with their use find optimal TMS bikes with respect to different stability criteria.

---

[1] i.e. an operator has a nontrivial Jordan normal form

[2] Frequently, the very multiple eigenvalue with the Jordan block in the complex plane is referred to as an exceptional point

2.3. Asymptotic stability of the TMS bike and the critical Froude number for the weaving motion

The TMS model (1), (2) is autonomous and nonconservative, containing dissipative, gyroscopic, potential and non-potential positional (circulatory [32], curl [33]) forces. Assuming the exponential solution $\sim \exp(s\tau)$ to the linear system (1) and computing $\det(\mathbf{M}s^2+\mathbf{V}s+\mathbf{P})$ we write the characteristic polynomial of the TMS bicycle model:

$$p(s) = a_0 s^4 + a_1 s^3 + a_2 s^2 + a_3 s + a_4, \tag{3}$$

with the coefficients

$$\begin{aligned} a_0 &= -(\zeta_H \tan\lambda_s - \chi_H + 1)\zeta_B^2, \\ a_1 &= \mathrm{Fr}(\zeta_B\chi_H - \zeta_H\chi_B)\zeta_B, \\ a_2 &= \mathrm{Fr}^2(\zeta_B - \zeta_H)\zeta_B - \zeta_B(\zeta_B + \zeta_H)\tan\lambda_s - (\chi_H - 1)(\mu\zeta_H - \zeta_B), \\ a_3 &= -\mathrm{Fr}(\chi_B - \chi_H)\zeta_B, \\ a_4 &= -\zeta_B \tan\lambda_s - \mu(\chi_H - 1). \end{aligned} \tag{4}$$

Applying the Lienard-Chipart version of the Routh-Hurwitz criterion [32,34] to the polynomial (3) yields for $\lambda_s > 0$ the following necessary and sufficient conditions for the asymptotic stability of the TMS bicycle

$$\begin{aligned} \chi_H &> 1 + \zeta_H \tan\lambda_s, \\ \chi_H &< 1 - \frac{\zeta_B}{\mu}\tan\lambda_s, \\ \chi_H &< \chi_B, \\ \zeta_H &> \zeta_B, \\ \mathrm{Fr} &> \mathrm{Fr}_c > 0, \end{aligned} \tag{5}$$

where the critical Froude number at the stability boundary is given by the expression

$$\mathrm{Fr}_c^2 = \frac{\zeta_B - \zeta_H}{\chi_B - \chi_H}\frac{\chi_B\chi_H}{\zeta_B\chi_H - \zeta_H\chi_B}\tan\lambda_s + \frac{\chi_H - 1}{\chi_B - \chi_H}\frac{\chi_H}{\zeta_B}\mu - \frac{\chi_H - 1}{\zeta_B\chi_H - \zeta_H\chi_B}\chi_B. \tag{6}$$

At $0 \le \mathrm{Fr} < \mathrm{Fr}_c$ the bicycle is unstable while at $\mathrm{Fr} > \mathrm{Fr}_c$ it is asymptotically stable. The critical value Fr_c is on the boundary between the domains of the asymptotic stability and dynamic instability (*weaving motion*, [19,20,27]). [3]

For instance, for the wheel base $w = 1m$ the design proposed in [27] is determined by

$$\lambda_s = \frac{5\pi}{180}rad,\;\; m_H = 1kg,\;\; m_B = 10kg,\;\; x_B = 1.2m,\;\; x_H = 1.02m,\;\; z_B = -0.4m,\;\; z_H = -0.2m. \tag{7}$$

With (7) we find from (6) the critical Froude number and the corresponding critical velocity

$$\mathrm{Fr}_c = 0.9070641497,\;\; v_c = 2.841008324m/s \tag{8}$$

that reproduce the original result obtained numerically in [27].

[3] Notice that in the recent work [35] a comprehensive analysis of the Lienard -Chipart conditions for the TMS-bicycle reduced self-stable designs to just two classes corresponding to either positive or negative angles λ_s and excluded backward stability for the TMS model. Here we limit our analysis to the $(\lambda_s > 0)$-class of the self-stable TMS bikes.

2.4. Minimizing the spectral abscissa of general TMS bikes

The criterion (5) guarantees asymptotic stability of the bicycle at $\mathrm{Fr} > \mathrm{Fr}_c$. However, the character of time dependence of the steering and leaning angles could be different at different points within the domain of asymptotic stability. Indeed, complex eigenvalues with negative real parts correspond to exponentially decaying oscillatory motions whereas negative real eigenvalues yield exponential decay of perturbations without oscillations. Recall that if all the eigenvalues of the system are real and negative, the system is heavily damped [36,37]. If we wish that the deviations from the straight vertical position of the heavily damped TMS bike riding along a straight line also quickly die out, we need to maximize the decay rates of the deviations in the following sense.

The abscissa of the polynomial $p(s)$ is the maximal real part of its roots

$$a(p) = \max\{\mathrm{Re}\, s : \ p(s) = 0\}.$$

Minimization of the spectral abscissa over the coefficients of the polynomial provides a polynomial with the roots that have minimal possible real parts (maximal possible decay rates). In the case of the system of coupled oscillators of the form (1) it is known that the global minimum of the spectral abscissa is $a_{min} = \omega_0$, where $\omega_0 = -\sqrt[4]{\frac{\det \mathbf{P}}{\det \mathbf{M}}}$ [38,39]. Knowing the coefficients of the characteristic polynomial (4) it is easy to find that for the TMS bicycle

$$\omega_0 = -\sqrt[4]{\frac{1}{\zeta_B^2}\frac{\zeta_B \tan\lambda_s + \mu(\chi_H - 1)}{\zeta_H \tan\lambda_s - (\chi_H - 1)}}. \tag{9}$$

Remarkably, if $s = \omega_0$ is the minimum of the spectral abscissa, it is the 4-fold root of the fourth-order characteristic polynomial (3) which is the quadruple negative real eigenvalue with the Jordan block of order 4 of the linear operator $\mathbf{M}s^2 + \mathbf{V}s + \mathbf{P}$ [17,38]. In this case the polynomial (3) takes the form

$$p(s) = (s - \omega_0)^4 = s^4 - 4s^3\omega_0 + 6s^2\omega_0^2 - 4s\omega_0^3 + \omega_0^4, \quad \omega_0^4 = \frac{a_4}{a_0} = \frac{\det \mathbf{P}}{\det \mathbf{M}}. \tag{10}$$

Comparing (3) and (10) we require that

$$\begin{aligned} a_1 &= \mathrm{Fr}(\zeta_B\chi_H - \zeta_H\chi_B)\zeta_B = -4\omega_0 a_0, \\ a_3 &= -\mathrm{Fr}(\chi_B - \chi_H)\zeta_B = -4\omega_0^3 a_0. \end{aligned}$$

Dividing the first equation by the second one, we get the relation

$$\frac{\zeta_B\chi_H - \zeta_H\chi_B}{\chi_B - \chi_H} = \frac{-1}{\omega_0^2}$$

that we resolve with respect to χ_B to obtain the following *design constraint* (or *scaling law*)

$$\chi_B = \frac{\omega_0^2\zeta_B - 1}{\omega_0^2\zeta_H - 1}\chi_H. \tag{11}$$

Another constraint follows from the requirement $a_2 = 6\omega_0^2 a_0$:

$$\mathrm{Fr}^2(\zeta_B - \zeta_H) + (6\omega_0^2\zeta_H\zeta_B - \zeta_B - \zeta_H)\tan\lambda_s = \zeta_B^{-1}(\chi_H - 1)(6\omega_0^2\zeta_B^2 + \mu\zeta_H - \zeta_B). \tag{12}$$

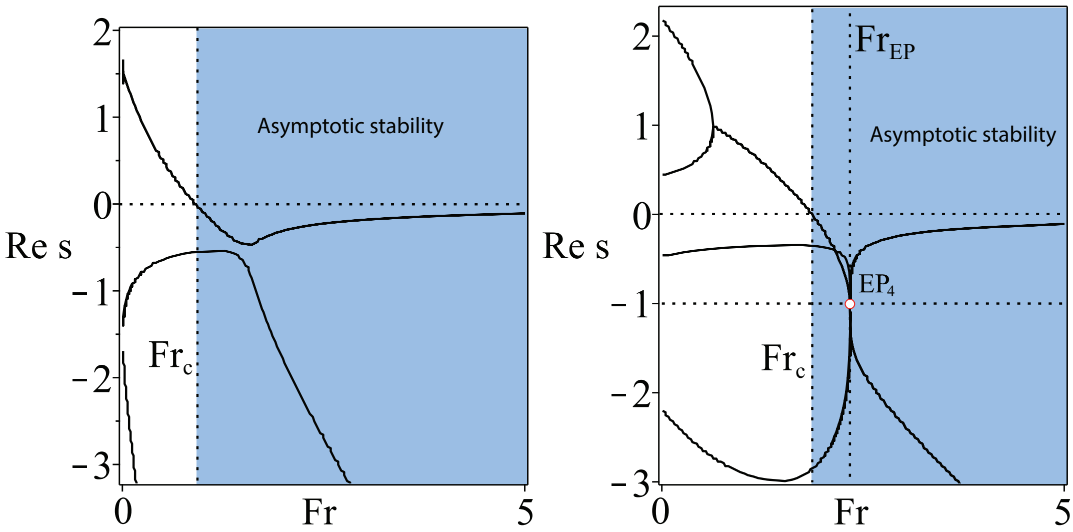

Figure 2. (Left) The growth rates for the benchmark TMS bicycle (7). (Right) The growth rates of the optimized TMS bicycle with $\zeta_B = -0.4$, $\zeta_H = -0.2$, $\chi_B = 1.19$, $\chi_H = 1.02$, $\mu = 20.84626701$, and $\lambda_s = 0.8514403685$ show that the spectral abscissa attains its minimal value $a_{min} = -1$ at $\mathrm{Fr}_{\mathrm{EP}} = 2.337214017$ at the real exceptional point of order 4, EP_4.

Let us optimize stability of the benchmark (7). Set, for example, $\omega_0 = -1$. Then, taking from the benchmark (7) the parameters $\zeta_B = -0.4$, $\zeta_H = -0.2$, and $\chi_H = 1.02$ we find from Eq. (11) that $\chi_B = 1.19$. With these values the constraint (12) is

$$-0.432\tan\lambda_s - 0.0272 + 0.08\mathrm{Fr}^2 + 0.004\mu = 0, \tag{13}$$

the relation (9) yields

$$0.368\tan\lambda_s - 0.02\mu - 0.0032 = 0, \tag{14}$$

and the characteristic polynomial evaluated at $s = -1$ results in the equation

$$0.192\tan\lambda_s - 0.0048 - 0.136\mathrm{Fr} + 0.08\mathrm{Fr}^2 - 0.016\mu = 0. \tag{15}$$

The system (13)–(15) has a unique solution with the mass ratio $\mu > 0$:

$$\mathrm{Fr} = 2.337214017, \quad \mu = 20.84626701, \quad \lambda_s = 0.8514403685.$$

This means that the optimized TMS bicycle attains the global minimum of the spectral abscissa at $\mathrm{Fr}_{EP} = 2.337214017$ where all four eigenvalues merge into a quadruple negative real eigenvalue $s = -1$ with the Jordan block, Fig. 2(right). This eigenvalue we call a *real exceptional point of order 4* and denote as EP_4. For comparison we show in Fig. 2(left) the growth rates of a generic benchmark TMS bicycle (7).

Why the location of the real EP_4 is important? In [17] it was shown that this exceptional point is a Swallowtail singularity on the boundary of the domain of heavy damping inside the domain of asymptotic stability of a system with two degrees of freedom. Furthermore, the global minimum of the spectral abscissa occurs exactly at the Swallowtail degeneracy. In [17] it was shown that the EP_4 'organizes' the asymptotic stability and its knowledge helps to locate other exceptional points governing stability exchange between modes of a coupled system. Below we demonstrate this explicitly for the TMS bikes with $\chi_H = 1$.

2.5. *Self-stable and heavily damped TMS bikes with $\chi_H = 1$*

2.5.1. The critical Froude number and its minimum

Why $\chi_H = 1$? First, both the benchmarks reported in [27] and their experimental realizations have $\chi_H \approx 1$. Second, this choice leads to a dramatic simplification without affecting generality of our consideration. Indeed, the expression (6) for the critical Froude number evaluated at $\chi_H = 1$ reduces to

$$\mathrm{Fr}_c^2 = \frac{\zeta_B - \zeta_H}{\zeta_B - \chi_B\zeta_H}\frac{\chi_B}{\chi_B - 1}\tan\lambda_s. \tag{16}$$

Choosing $\chi_H = 1$ automatically makes Fr_c and the stability conditions (5) independent on the mass ratio μ. Additionally, the criteria (5) imply $\chi_B > 1$ and $|\zeta_B| > |\zeta_H|$.

Therefore, choosing $\chi_H = 1$ reduces the dimension of the parameter space from 7 to 5. The self-stability of the $(\chi_H = 1)$–bike depends just on Fr, χ_B, ζ_H, ζ_B, and λ_s.

Given ζ_H, ζ_B, and λ_s find the minimum of the critical Froude number (16) as a function of χ_B. It is easy to see that the minimum is attained at

$$\chi_B = \sqrt{\frac{\zeta_B}{\zeta_H}} \tag{17}$$

and its value is equal to

$$\mathrm{Fr}_{min} = \sqrt{\frac{\sqrt{|\zeta_B|} + \sqrt{|\zeta_H|}}{\sqrt{|\zeta_B|} - \sqrt{|\zeta_H|}}\tan\lambda_s}. \tag{18}$$

These results suggest that all the critical parameters for the $(\chi_H = 1)$–bike can be expressed in a similar elegant manner by means of ζ_H, ζ_B, and λ_s only. Let us check these expectations calculating the location of the real exceptional point EP_4 for the $(\chi_H = 1)$–bike.

2.5.2. Exact location of the real exceptional point EP_4

Indeed, with $\chi_H = 1$ the expression (9) for the real negative quadruple eigenvalue at EP_4 yields

$$\omega_0 = -\sqrt[4]{\frac{1}{\zeta_B\zeta_H}}. \tag{19}$$

The design constraint (11) reduces to the scaling law

$$\chi_B = \sqrt{\frac{\zeta_B}{\zeta_H}} \tag{20}$$

which is nothing else but the minimizer (17) of the critical Froude number ! Solving simultaneously the equation (12) and the equation $p(\omega_0) = 0$ we find explicitly the second design constraint that determines $\tan\lambda_s$ at EP_4:

$$\tan\lambda_s = \frac{\omega_0^2(\zeta_B - \zeta_H)}{16\zeta_H}\frac{(\zeta_B + \zeta_H)\omega_0^2 - 6}{(\zeta_B + \zeta_H)\omega_0^2 - 2}. \tag{21}$$

Finally, from the same system of equations we find that the Froude number at EP_4, $\mathrm{Fr}_{\mathrm{EP}_4}$, is a root of the quadratic equation

$$\left(\omega_0^2\zeta_B - 1\right)\mathrm{Fr}_{\mathrm{EP}_4}^2 + 2\omega_0^3\zeta_B\mathrm{Fr}_{\mathrm{EP}_4} - (\omega_0^2\zeta_B + 1)\tan\lambda_s = 0, \tag{22}$$

where ω_0 is given by equation (19) and $\tan\lambda_s$ by equation (21).

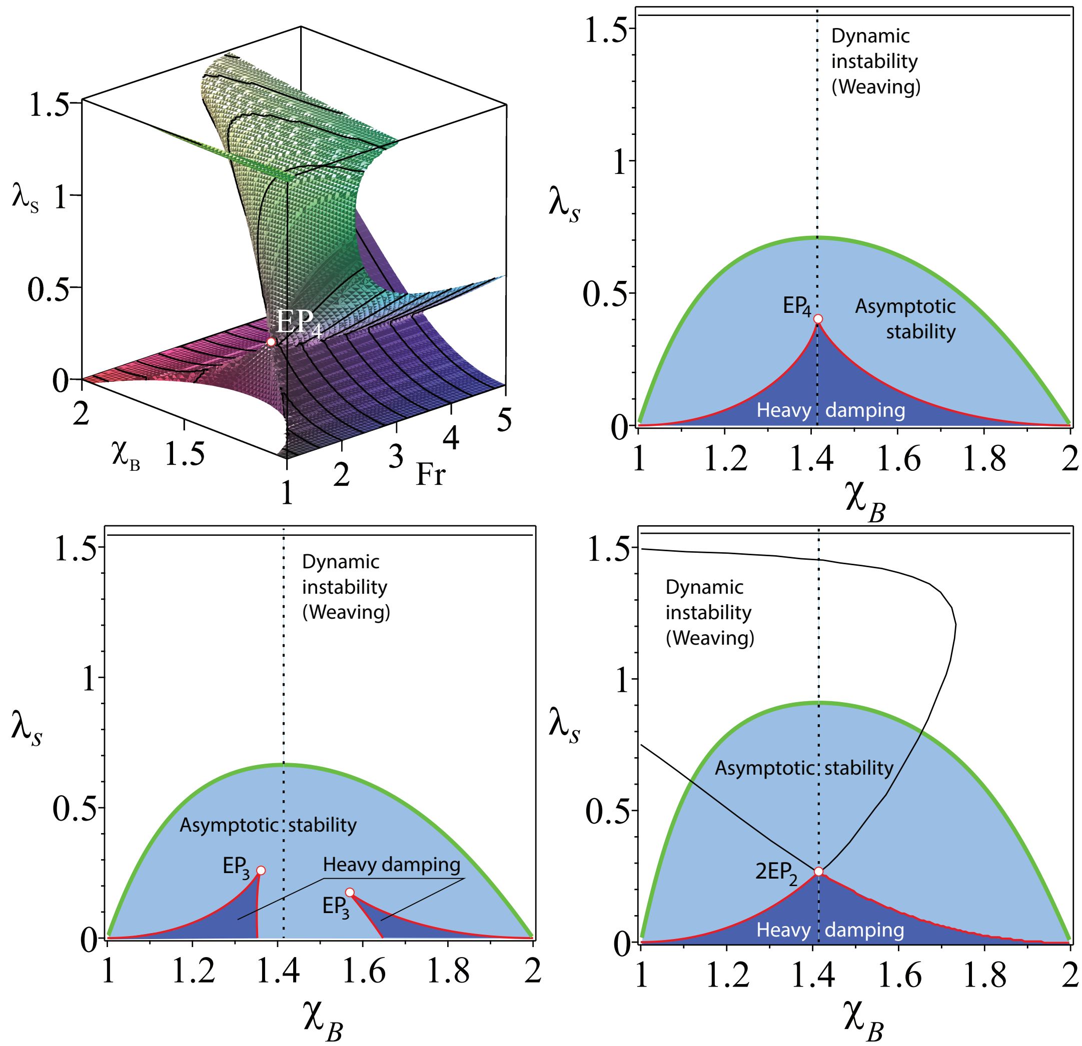

Figure 3. (Upper left) The discriminant surface of the characteristic polynomial of the TMS-bike with $\chi_H = 1$, $\zeta_H = -0.2$, and $\zeta_B = -0.4$ showing the Swallowtail singularity at EP_4. The cross-section of the domain of asymptotic stability and the discriminant surface at (upper right) $Fr = Fr_{EP_4} = \frac{3\sqrt{110\sqrt{2}-120}}{8}$, (lower left) $Fr = Fr_{EP_4} - 0.1$ and (lower right) $Fr = Fr_{EP_4} + 0.5$.

Table 2. TMS bike designs with $\chi_H = 1$

Bike	χ_H	χ_B	ζ_H	ζ_B	ω_0	λ_s (rad.)	Fr_c	Fr_{EP}
EP_4	1	$\sqrt{2}$	-0.2	-0.4	$-\frac{\sqrt{5}}{\sqrt[4]{2}}$	$\arctan\left(\frac{15}{4} - \frac{75}{32}\sqrt{2}\right)$	$\frac{\sqrt{30\sqrt{2}+120}}{8}$	$\frac{3\sqrt{110\sqrt{2}-120}}{8}$
$2EP_2$	1	$\sqrt{2}$	-0.2	-0.4	$-\frac{\sqrt{5}}{\sqrt[4]{2}}$	$\arctan\left(\frac{15}{4} - \frac{75}{32}\sqrt{2}\right) - 0.05$	≈ 1.482682090	≈ 2.257421384
CEP_2	1	$\sqrt{2}$	-0.2	-0.4	$-\frac{\sqrt{5}}{\sqrt[4]{2}}$	$\arctan\left(\frac{15}{4} - \frac{75}{32}\sqrt{2}\right) + 0.80$	≈ 3.934331969	≈ 4.103508160

Let us take $\zeta_H = -0.2$ and $\zeta_B = -0.4$ as in the benchmark (7). Then (20), (21), and (22) locate the EP_4 in the space of the parameters giving (Table 2)

$$\chi_B = \sqrt{2}, \quad \tan\lambda_s = \frac{15}{4} - \frac{75}{32}\sqrt{2}, \quad Fr_{EP_4} = \frac{3\sqrt{110\sqrt{2}-120}}{8} \approx 2.236317517.$$

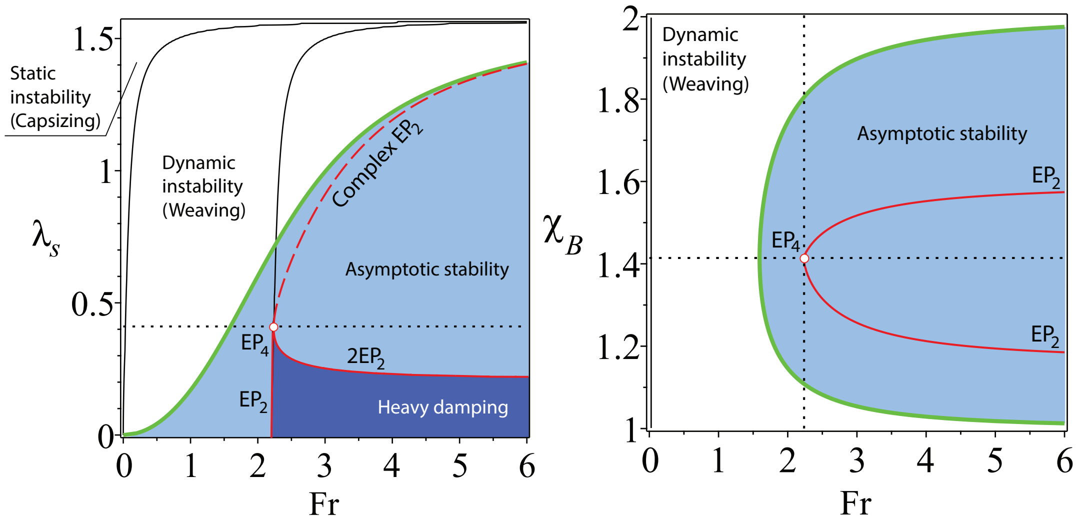

Figure 4. $\chi_H = 1$, $\zeta_H = -0.2$, and $\zeta_B = -0.4$. (Left) For $\chi_B = \sqrt{2}$ the boundary between the domains of weaving and asymptotic stability in the (Fr, λ_s) - plane shown together with the domain of heavy damping that has a cuspidal point corresponding to a negative real eigenvalue $\omega_0 = -\sqrt[4]{\frac{25}{2}}$ with the Jordan block of order four (EP_4). The EP_4 belongs to a curve (23) that corresponds to (dashed part) conjugate pairs of double complex eigenvalues with the Jordan block of order two (complex EP_2) and (solid part) to couples of double real negative eigenvalues with the Jordan block of order two ($2EP_2$). (Right) The same in the (Fr, χ_B)–plane at $\lambda_s = \arctan\left(\frac{15}{4} - \frac{75}{32}\sqrt{2}\right)$ rad. The domain of heavy damping degenerates into a singular point - the Swallowtail singularity.

2.5.3. Discriminant surface and the EP-set

The located EP_4 corresponds to a quadruple negative real eigenvalue $s = \omega_0 = -\frac{\sqrt{5}}{\sqrt[4]{2}}$. It is known that EP_4 is the Swallowtail singular point on the discriminant surface of the fourth-order characteristic polynomial [17]. In Fig. 3 the discriminant surface is plotted in the $(\mathrm{Fr}, \chi_B, \lambda_s)$ –space for the TMS-bike with $\chi_H = 1$, $\zeta_H = -0.2$, and $\zeta_B = -0.4$ showing the Swallowtail singular point with the position specified by the first line of the Table 2. The discriminant surface has two cuspidal edges as well as the line of self-intersection branching from the EP_4. These singularities belong to the boundary of a domain with the shape of a trihedral spire. This is the domain of heavy damping. In its inner points all the eigenvalues are real and negative [17].

We see that the line of self-intersection lies in the plane $\chi_B = \sqrt{\frac{\zeta_B}{\zeta_H}}$. Restricted to this plane (parameterized by Fr and λ_s) the discriminant of the characteristic polynomial (3) simplifies and provides the following expression for the curve that contains the line of self-intersection of the discriminant surface

$$\mathrm{Fr} = \frac{\omega_0^2\zeta_B - 1}{\omega_0^2\zeta_B + 1}\frac{2\tan\lambda_s}{\sqrt{\omega_0^4\zeta_B + 4\tan\lambda_s\frac{\omega_0^2\zeta_B - 1}{\omega_0^2\zeta_B + 1}}}. \tag{23}$$

In Fig. 4(left) the curve (23) is plotted for $\chi_H = 1$, $\zeta_H = -0.2$, $\zeta_B = -0.4$ and $\chi_B = \sqrt{2}$ in the (Fr, λ_s)–plane. A point where this curve has a vertical tangent is the Swallowtail singularity or EP_4. The part of the curve below the EP_4 is a line of self-intersection of the discriminant surface corresponding to a pair of different negative double real eigenvalues with the Jordan block, i.e. to a couple of real exceptional points which we denote as $2EP_2$.

The curve (23) continues, however, also above the EP_4. This part shown by a dashed line in Fig. 4(left) is the set corresponding to conjugate pairs of complex double eigenvalues with the Jordan block, or complex exceptional points that we denote as CEP_2. Since the curve (23) is a location of three

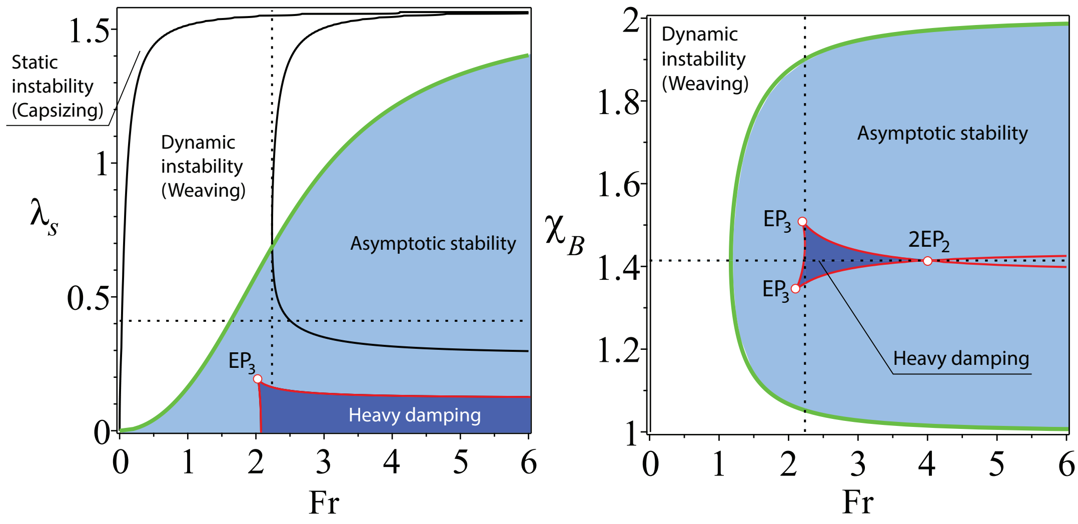

Figure 5. $\chi_H = 1$, $\zeta_H = -0.2$, and $\zeta_B = -0.4$. (Left) For $\chi_B = \sqrt{2} - 0.1$ the boundary between the domains of weaving and asymptotic stability in the (Fr, λ_s) - plane shown together with the domain of heavy damping that has a cusp corresponding to a negative real eigenvalue with the Jordan block of order three (EP_3). The EP_3 belongs to the cuspidal edge of the swallowtail surface bounding the domain of heavy damping. (Right) The same in the (Fr, χ_B)-plane at $\lambda_s = \arctan\left(\frac{15}{4} - \frac{75}{32}\sqrt{2}\right) - 0.18$ rad. Notice the cuspidal EP_3-points and the self intersection at the $2EP_2$ point on the boundary of the domain of heavy damping.

types of exceptional points we call it the *EP-set*. Notice that the codimension of the EP-set is 2 and by this reason its location by numerical approaches is very non-trivial.

2.5.4. Location of the EP-set and stability optimization

What the location of the EP-set means for the stability of the TMS bike? Drawing the domain of asymptotic stability together with the discriminant surface and the EP-set in the same plot, we see that the EP-set lies entirely in the domain of asymptotic stability, Fig. 4. The $2EP_2$ part of the EP-set bounds the domain of heavy damping in the plane $\chi_B = \sqrt{\frac{\zeta_B}{\zeta_H}} = \sqrt{2}$.

Look now at the cross-sections of the asymptotic stability domain and the discriminant surface in the (χ_B, λ_s)–plane, Fig. 3. Remarkably, the value $\chi_B = \sqrt{\frac{\zeta_B}{\zeta_H}} = \sqrt{2}$ is a maximizer of the steer axis tilt λ_s both at the onset of the weaving instability and at the boundary of the domain of heavy damping. In the latter case the maximum is always attained at a singular point in the EP-set: either at EP_4 when $\mathrm{Fr} = \mathrm{Fr}_{EP_4}$ or at $2EP_2$ when $\mathrm{Fr} > \mathrm{Fr}_{EP_4}$. The global maximum of the steer axis tilt on the boundary of the domain of heavy damping is attained exactly at EP_4 which is also the point where the spectral abscissa attains its global minimum. Taking into account that $\chi_B = \sqrt{\frac{\zeta_B}{\zeta_H}} = \sqrt{2}$ is a minimizer of the critical Froude number that is necessary for asymptotic stability, we conclude that the both of the design constraints, (20) and (21), play a crucial part in the self-stability phenomenon:

The most efficient self-stable TMS bikes are those that have better chance to operate in the heavy damping domain and simultaneously have the minimal possible spectral abscissa. In the case when $\chi_H = 1$, these bikes should necessarily follow the scaling laws

$$\chi_B = \sqrt{\frac{\zeta_B}{\zeta_H}} \quad \textit{and} \quad 0 < \tan\lambda_s \leq \frac{\omega_0^2(\zeta_B - \zeta_H)}{16\zeta_H}\frac{(\zeta_B + \zeta_H)\omega_0^2 - 6}{(\zeta_B + \zeta_H)\omega_0^2 - 2}, \quad \textit{where} \quad \omega_0 = -\sqrt[4]{\frac{1}{\zeta_B \zeta_H}}. \tag{24}$$

Even in the case of an approximate scaling law $\chi_B \approx \sqrt{\frac{\zeta_B}{\zeta_H}}$ the domain of heavy damping is large enough, Fig. 5, suggesting that the formulated principle produces sufficiently robust design of self-stable TMS bikes.

2.5.5. Mechanism of self-stability and CEP_2 as a precursor to bike's weaving

What happens with the stability of TMS bicycles that have large steer axis tilt? To answer this question let us look at the movement of eigenvalues in the complex plane at different λ_s and χ_B as the Froude number increases from 0 to 5, Fig. 6. At $\mathrm{Fr} = 0$ the bicycle is effectively an inverted pendulum which is statically unstable (capsizing instability [20]) with two real negative eigenvalues and two real positive eigenvalues. As Fr increases the positive eigenvalues move towards each other along the real axis. The same happens (at a slower rate) with the negative eigenvalues. Eventually, the positive real eigenvalues merge into a double real eigenvalue $s = -\omega_0 > 0$. The subsequent evolution of eigenvalues depends on χ_B and λ_s.

If $\chi_B = \sqrt{\frac{\zeta_B}{\zeta_H}} = \sqrt{2}$ then with the further increase in Fr the double eigenvalue $s = -\omega_0 > 0$ splits into a conjugate pair of complex eigenvalues with positive real parts causing weaving instability. This pair evolves along a circle $(\mathrm{Re}\, s)^2 + (\mathrm{Im}\, s)^2 = \omega_0^2$ and crosses the imaginary axis exactly at $\mathrm{Fr} = \mathrm{Fr}_c$ given by equation (16), which yields the asymptotic stability of the bicycle.

The further evolution of the eigenvalues depends on the steer axis tilt λ_s, Fig. 6. If λ_s satisfies the constraint (21) then the complex eigenvalues with the negative real parts moving along the circle approach the real axis and meet the two negative real eigenvalues exactly at $\mathrm{Fr} = \mathrm{Fr}_{\mathrm{EP}_4}$ forming a quadruple negative real eigenvalue $s = \omega_0$, i.e. the real exceptional point EP_4. At this moment all the four eigenvalues are shifted as far as possible to the left from the imaginary axis, which corresponds to the global minimum of the spectral abscissa, Fig. 6(upper row). Further increase in Fr leads to the splitting of the multiple eigenvalue into a quadruplet of complex eigenvalues with negative real parts (decaying oscillatory motion) and to the increase in the spectral abscissa.

If $\chi_B = \sqrt{\frac{\zeta_B}{\zeta_H}} = \sqrt{2}$ and λ_s is smaller than the value specified by (21), then the pair moving along the circle reaches the real axis faster than the negative real eigenvalues meet each other, Fig. 6(middle row). Then, the complex eigenvalues merge into a double negative real eigenvalue $s = \omega_0$ which splits into two negative real ones that move along the real axis in the opposite directions. At these values of Fr the system has four simple negative real eigenvalues, which correspond to heavy damping. The time evolution of all perturbations is then the monotonic exponential decay, which is favorable for the bike robustness. At $\mathrm{Fr} = \mathrm{Fr}_{EP}$ which is determined by the equation (23) two real negative double eigenvalues originate simultaneously marking formation of the $2EP_2$ singularity on the boundary of the domain of heavy damping. Further increase in Fr yields splitting of the multiple eigenvalues into two pairs of complex eigenvalues with negative real parts (decaying oscillatory motion).

If $\chi_B = \sqrt{\frac{\zeta_B}{\zeta_H}} = \sqrt{2}$ and λ_s is larger than the value specified by (21), then the pair moving along the circle do it so slowly that the real negative eigenvalues manage to merge into a double negative real eigenvalue $s = \omega_0$ and then become a pair of two complex eigenvalues evolving along the same circle towards the imaginary axis, Fig. 6(lower row). The pairs of complex eigenvalues meet on the circle at $\mathrm{Fr} = \mathrm{Fr}_{\mathrm{EP}}$ which is determined by the equation (23), i.e. at a point of the EP-set corresponding to a pair of complex exceptional points EP_2. After the collision the eigenvalues split into four complex eigenvalues with the real parts.

From this analysis we see that λ_s indeed determines the balance of the rate of stabilization of unstable modes and the rate of destabilization of unstable modes. The former is larger when λ_s is smaller than the value specified by (21) and the latter is larger when λ_s exceeds the value specified by (21) thus confirming the design principle (24). The perfect balance corresponds to the angle λ_s specified by (21), which yields global minimization of the spectral abscissa.

When $\chi_B \neq \sqrt{\frac{\zeta_B}{\zeta_H}}$, then the eigenvalues evolve close to the circle $(\mathrm{Re}\, s)^2 + (\mathrm{Im}\, s)^2 = \omega_0^2$ but this evolution again differs for different values of λ_s. If for λ_s smaller than the value specified by (21) the

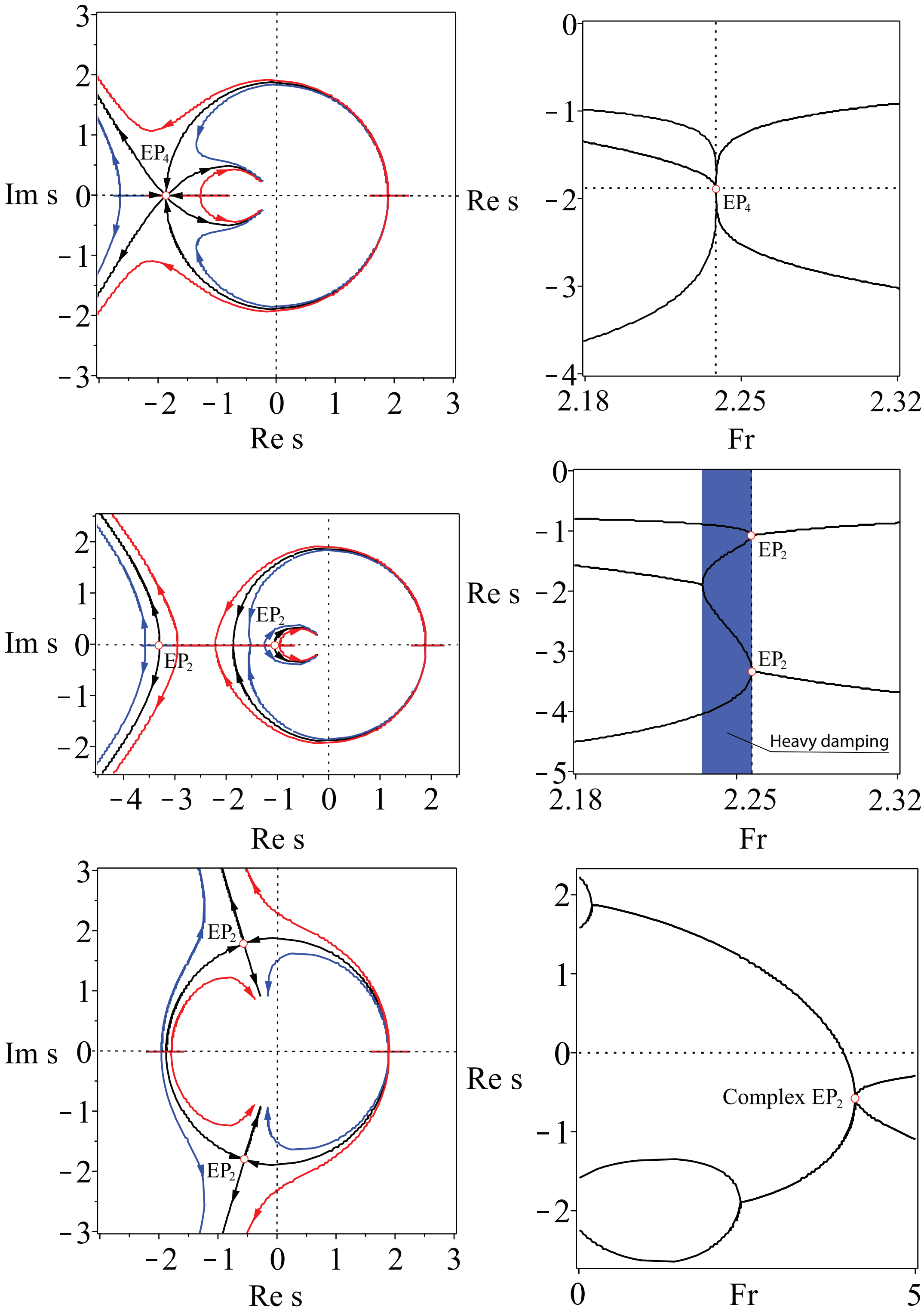

Figure 6. $\chi_H = 1$, $\zeta_H = -0.2$, $\zeta_B = -0.4$. Stabilization of the TMS bike as Fr is increasing from 0 to 5 for (upper row) $\lambda_s = \arctan\left(\frac{15}{4} - \frac{75}{32}\sqrt{2}\right)$ rad., (middle row) $\lambda_s = \arctan\left(\frac{15}{4} - \frac{75}{32}\sqrt{2}\right) - 0.05$ rad., and (lower row) $\lambda_s = \arctan\left(\frac{15}{4} - \frac{75}{32}\sqrt{2}\right) + 0.8$ rad. The eigenvalue curves are shown for (black) $\chi_B = \sqrt{2}$, (blue) $\chi_B = \sqrt{2} - 0.01$, and (red) $\chi_B = \sqrt{2} + 0.01$ in the upper and middle rows and for (black) $\chi_B = \sqrt{2}$, (blue) $\chi_B = \sqrt{2} - 0.1$, and (red) $\chi_B = \sqrt{2} + 0.1$ in the lower row. Notice the existence at $\chi_B = \sqrt{2}$ of (upper row) a real exceptional point EP_4, (middle row) a couple of real exceptional points EP_2, and (lower row) a couple of complex exceptional points EP_2 and repelling of eigenvalue curves near EPs when $\chi_B \neq \sqrt{2}$.

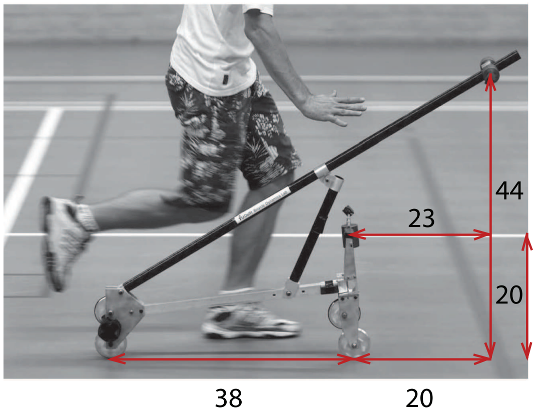

Figure 7. Experimental realization of a self-stable TMS bicycle design found by trials and errors in [18,27] with $\chi_B = 1.526$, $\chi_H = 0.921$, $\zeta_B = -1.158$, $\zeta_H = -0.526$ approximately fits the scaling law (20). Indeed, $\sqrt{\frac{\zeta_B}{\zeta_H}} = 1.484$ is close to $\chi_B = 1.526$.

eigenvalue evolution remains qualitatively the same, as is evident from Fig. 6(middle row), for λ_s larger than the value specified by (21) the eigenvalues experience strong repulsion near the location of CEP_2, i.e. when the parameters evolve close to the EP-set of complex exceptional points. Such behavior of eigenvalues in dissipative systems permanently intrigues many researchers. For instance, Jones [13] remarked in the context of the stability of the plane Poiseuille flow that "unfortunately, it is quite common for an eigenvalue which is moving steadily towards a positive growth rate to suffer a sudden change of direction and subsequently fail to become unstable; similarly, it happens that modes which initially become more stable as [the Reynolds number] increases change direction and subsequently achieve instability. *It is believed that these changes of direction are due to the nearby presence of multiple-eigenvalue points.*" This 'nearby presence' of complex exceptional points is elusive unless we manage to locate the EP-set. For the TMS bike we have obtained this set in the explicit form given by equations (19), (20), and (23). Dobson et al. [14] posed a question "is strong modal resonance a precursor to [oscillatory instability]?" The strong modal resonance is exactly the interaction of eigenvalues at CEP_2 shown in Fig. 6(lower row). Knowing the exact location of the EP-set of complex exceptional points we can answer affirmatively to the question of Dobson et al. Indeed, the complex EP-set shown as a dashed curve in Fig. 4(left) tends to the boundary of asymptotic stability as $\lambda_s \to \frac{\pi}{2}$. This means that the CEP_2 in Fig. 6(lower row) come closer to the imaginary axis at large λ_s and even small perturbations in χ_B can turn the motion of eigenvalues back to the right hand side of the complex plane and destabilize the system. Fig. 6(lower row) also demonstrates the selective role of the scaling law $\chi_B = \sqrt{\frac{\zeta_B}{\zeta_H}}$ in determining which mode becomes unstable. The conditions $\chi_B > \sqrt{\frac{\zeta_B}{\zeta_H}}$ and $\chi_B < \sqrt{\frac{\zeta_B}{\zeta_H}}$ affect modes with the higher or the lower frequency, respectively. In fact, in the limit $\lambda_s \to \frac{\pi}{2}$ the dissipative system becomes close to a system with a Hamiltonian symmetry of the spectrum. This could be a reversible, Hamiltonian or PT-symmetric system [9,10,12,32] which is very sensitive to perturbations destroying the fundamental symmetry and therefore can easily be destabilized.

2.5.6. How the scaling laws found match the experimental TMS bike realization

In Fig. 7 we show the photograph of the experimental TMS bike from the work [27], see also [18]. If we measure the lengths of the bike right on the photo, we can deduce that for this realization the design parameters are $\chi_B = 1.526$, $\chi_H = 0.921$, $\zeta_B = -1.158$, $\zeta_H = -0.526$. Hence,

$$\sqrt{\frac{\zeta_B}{\zeta_H}} = 1.484 \approx \chi_B = 1.526,$$

which means that the scaling law (20) is matched pretty well. This leads us to the conclusion that the trial-and-error engineering approach to the design of a self-stable TMS bike reported in [27] has eventually produced the design that is close to the optimally stable with respect to at least three different criteria: minimization of the spectral abscissa, minimization of Fr_c and maximization of the domain of heavy damping. Indeed, our scaling laws (20) and (21) directly follow from the exact optimal solutions to these problems.

3. Conclusions

We have found new scaling laws for the two-mass-skate (TMS) bicycle that lead to the design of self-stable machines. These scaling laws optimize stability of the bicycle by several different criteria simultaneously. The matching of the theoretical scaling laws to the parameters of the TMS bikes realization demonstrates that the trial-and-error engineering of the bikes selects the most robustly stable species and thus empirically optimizes the bike stability. We have found the optimal solutions directly from the analysis of the sets of exceptional points of the TMS bike model with the help of a general result on the global minimization of the spectral abscissa at an exceptional point of the highest possible order. We stress that all previous results on the self-stability of bicycles even in the linear case have been obtained numerically.

Acknowledgments: Support from a Vice Chancellor's Research Fellowship at Northumbria University is gratefully acknowledged.

Conflicts of Interest: The author declares no conflict of interest.

1. Bender, C. M., Berntson, B. K., Parker, D., Samuel, E. Observation of PT phase transition in a simple mechanical system. *Am. J. Phys.*, **2013**, *81*, 173–179.
2. Xu, X.-W., Liu, Y.-X., Sun, C.-P., Li, Y. Mechanical PT symmetry in coupled optomechanical systems. *Phys. Rev A* **2015**, *92*, 013852.
3. Schindler, S., Lin, Z., Lee, J. M., Ramezani, H., Ellis, F. M., Kottos, T. PT symmetric electronics. *J. Phys. A: Math. Theor.* **2012**, *45*, 444029.
4. Freitas, P. On some eigenvalue problems related to the wave equation with indefinite damping. *J. Diff. Equ.*, **1996**, *127*, 320–335.
5. Freitas, P., Zuazua, E. Stability results for the wave equation with indefinite damping. *J. Diff. Equ.*, **1996**, *132*, 338–353.
6. Freitas, P., Grinfeld, M., Knight, P. A. Stability of finite-dimensional systems with indefinite damping. *Adv. Math. Sci. Appl.*, **1997**, *7*, 437–448.
7. Freitas P. Quadratic matrix polynomials with Hamiltonian spectrum and oscillatory damped systems. *Z. Angew. Math. Phys.*, **1999**, *50*, 64–81.
8. Kliem W., Pommer C. Indefinite damping in mechanical systems and gyroscopic stabilization. *Z. Angew. Math. Phys.*, **2009**, *60*, 785–795.
9. Kirillov, O. N. PT symmetry, indefinite damping and dissipation-induced instabilities. *Phys. Lett. A*, **2012**, *376(15)*, 1244–1249.
10. Kirillov, O. N. Stabilizing and destabilizing perturbations of PT symmetric indefinitely damped systems. *Phil. Trans. R. Soc. A*, **2013**, *371*, 20120051.

11. Kirillov, O. N. Exceptional and diabolical points in stability questions. *Fortschritte der Physik – Progress in Physics*, **2013**, *61*(2–3), 205–224.
12. Kirillov, O. N. Singular diffusionless limits of double-diffusive instabilities in magnetohydrodynamics. *Proc. R. Soc. A*, **2017**, *473(2205)*, 20170344.
13. Jones, C. A. Multiple eigenvalues and mode classification in plane Poiseuille flow. *Quart. J. Mech. Appl. Math.*, **1988**, *41*, 363–382.
14. Dobson, I., Zhang, J., Greene, S., Engdahl, H., Sauer, P. W. Is strong modal resonance a precursor to power system oscillations? *IEEE Trans. Circ. Syst. I*, **2001**, *48*, 340–349.
15. Friedland, S. Simultaneous similarity of matrices. *Advances in Mathematics* **1983**, *50*, 189–265.
16. Christensen, E. On invertibility preserving linear mappings, simultaneous triangularization and Property L. *Lin. Alg. Appl.* **1999**, *301*, 153–170.
17. Kirillov, O. N., Overton, M. L. Robust stability at the swallowtail singularity. *Frontiers in Physics*, **2013**, *1*, 24.
18. Borrell, B. Physics on two wheels. *Nature*, **2016**, *535*(7612), 338–341.
19. Meijaard, J. P., Papadopoulos, J. M., Ruina, A., Schwab, A. L. Linearized dynamics equations for the balance and steer of a bicycle: a benchmark and review. *Proc. R. Soc. A*, **2007**, *463*, 1955–1982.
20. Sharp, R. S. On the stability and control of the bicycle. *Appl. Mech. Rev.*, **2008**, *61*, 060803-1.
21. Meijaard, J. P., Papadopoulos, J. M., Ruina, A., Schwab, A. L. Historical review of thoughts on bicycle self-stability. **2011**, Cornell University, Ithaca, NY.
22. Boyer, F., Porez, M., Mauny, J. Reduced dynamics of the non-holonomic Whipple bicycle. *J Nonlinear Sci.*, **2018**.
23. Borisov, A. V., Mamaev, I. S., Bizyaev, I. A. Dynamical systems with non-integrable constraints, vakonomic mechanics, sub-Riemannian geometry, and non-holonomic mechanics. *Russian Math. Surveys*, **2017**, **72**(5), 783–840.
24. Levi, M., S. Tabachnikov. On bicycle tire tracks geometry, hatchet planimeter, Menzin's conjecture, and oscillation of unicycle tracks. *Exp. Math.* **2009**, *18*, 173–186.
25. Levi, M. Schrödinger's equation and "bike tracks" – A connection. *J. Geom. Phys.*, **2017**, *115*, 124–130.
26. Bor, G., Levi, M., Perline, R., Tabachnikov, S. Tire tracks and integrable curve evolution. *Internat. Math. Res. Not.*, **2018**, rny087.
27. Kooijman, J. D. G., Meijaard, J. P., Papadopoulos, J. M., Ruina, A., Schwab, A. L. A bicycle can be self-stable without gyroscopic or caster effects. *Science*, **2011**, *332(6027)*, 339–342.
28. Ricci, F., Frosali, G. A symbolic method for the analysis of a nonlinear Two-Mass-Skate model. *arXiv: 1611.07796*, **2016**.
29. Collins, S., Ruina, A., Tedrake, R. and Wisse, M. Efficient bipedal robots based on passive-dynamic walkers. *Science*, **2005**, *307*, 1082–1085.
30. Borisov, A. V., Kilin, A. A., Mamaev, I. S. On the Hadamard-Hamel problem and the dynamics of wheeled vehicles. *Reg. Chaot. Dyn.*, **2015**, *20*(6), 752–766.
31. Lyapunov, A. M. The general problem of the stability of motion (translated into English by A. T. Fuller). *Int. J. Control*, **1992**, *55*, 531–773.
32. Kirillov, O. N. *Nonconservative Stability Problems of Modern Physics.* De Gruyter: Berlin, Boston, 2013.
33. Berry, M. V., Shukla. P. Curl force dynamics: symmetries, chaos and constants of motion. *New J. Phys.*, **2016**, *18*, 063018.
34. Kirillov, O. N. Classical results and modern approaches to nonconservative stability. Ch. 4. In: *D. Bigoni and O. Kirillov (eds.), Dynamic Stability and Bifurcation in Nonconservative Mechanics*, CISM International Centre for Mechanical Sciences 586, Springer, Berlin, 2018, pp. 129–190.
35. Austin Sydes, G. L. *Self-stable bicycles.* BSc (Hons) Mathematics final year project report. Northumbria University, Newcastle upon Tyne, UK, 2018.
36. Barkwell, L., Lancaster, P. Overdamped and gyroscopic vibrating systems. *J. Appl. Mech.*, **1992**, *59*, 176–181.
37. Veselic, K. *Damped Oscillations of Linear Systems: A Mathematical Introduction.* Springer: Berlin, Germany, 2011.
38. Freitas, P., Lancaster, P. On the optimal value of the spectral abscissa for a system of linear oscillators. *SIAM J. Matrix Anal. Appl.*, **1999**, *21*, 195–208.
39. Blondel, V. D., Gurbuzbalaban, M., Megretski, A., Overton, M. L. Explicit solutions for root optimization of a polynomial family with one affine constraint. *IEEE Trans. Autom. Control*, **2012**, *57*(12), 3078–3089.